Fully Three-dimensional Radial Visualization

Yifan Zhu, Fan Dai and Ranjan Maitra

Abstract

We develop methodology for three-dimensional (3D) radial visualization (RadViz) of multidimensional datasets. Our tool is called RadViz3D and extends the classical two-dimensional (2D) RadViz that visualizes multivariate data in the 2D plane by mapping every observation to a point inside the unit circle. We show that distributing anchor points uniformly on the 3D unit sphere provides the best visualization with minimal artificial visual correlation for data with uncorrelated variables. However, anchor points can be placed exactly equi-distant from each other only for the five Platonic solids. We provide equi-distant anchor points for these five settings, and approximately equi-distant anchor points via a Fibonacci grid for the other cases. Our methodology, implemented in the R package radviz3d, makes fully 3D RadViz possible and is shown to improve clarity of this nonlinear display technique on simulated and real datasets.

Index Terms

CARP, crabs, generalized radial visualization, generalized overlap, MixSim, normalized radial visualization, olive oils dataset, star coordinates plot, Viz3D, wine dataset

I. Introduction

Graphical display of multivariate data is important to obtain insight into their properties and similarity or distinctiveness of different groups [1]. The goal of effective visualization is to map multi-dimensional observations to a lower-dimensional space, with the reduced display conveying information on the characteristics as faithfully as possible.

Continuous multivariate data are displayed in many ways [2] (e.g. starplots [3], Chernoff faces [4], parallel coordinate plots [5], [6], surveyplots [7], Andrews' curves [8], [9], biplots [10], star coordinate plots [11], Uniform Manifold Approximation and Projections (UMAP) [12]), but our focus in this short technical note is on improving the nonlinear display called radial visualization or RadViz [13], [14], [15], [16] that projects data onto a circle using Hooke's law. Here, p-dimensional observations are projected onto the 2D plane using p anchor points arranged to be on the perimeter of a circle. This representation places each observation at the center of the circle that is then pulled by springs in the directions of the p anchor points while being balanced by forces relative to the coordinate values. Observations with similar relative values across all attributes are placed close to the center while the others are closer to anchor points corresponding to the coordinates with higher relative values. However, there is loss of information [17] in RadViz which maps a p-dimensional point to 2D. This loss worsens with increasing p, but may potentially be alleviated by extending it to 3D. The Viz3D approach [17] extends 2D RadViz (henceforth, RadViz2D) by simply adding to the 2D projection a third dimension that is constant for all features. Viz3D's improvement over RadViz2D is by design limited, so we investigate the possibility of developing a truly 3D extension of RadViz.

One challenge of extending RadViz from two to three dimensions is that a 3D sphere can be exactly divided into p regions of equal volumes only for the Platonic solids. However, Section II shows that placing equi-spaced anchor points is necessary to reduce artificially induced correlation between variables. So, for other p, Section II uses a Fibonacci grid method to develop an approximate solution. We call our method RadViz3D and illustrate in Section III its ability to more accurately display structure in simulated and real datasets than RadViz2D or Viz3D. The main paper concludes with some discussion. We also have an online supplemental HTML resource at https://fanne-stat.github.io/RadViz3DExperiments/supplement_jcgs.html that allows the reader to more fully experience the benefits of RadViz3D (and Viz3D) on our examples.

II. METHODOLOGY

A. Generalized radial visualization

We first define generalized radial visualization (GRadViz) as a natural extension of the classic RadViz2D that maps $X = (X_1, X_2, \dots, X_p)^{\top} \in \mathcal{R}^p$ to a 2D point using

$$\Psi^{\bullet}(X;U) = \frac{UX}{\mathbf{1}_{n}^{\top}X},\tag{1}$$

Y. Zhu and R. Maitra are with the Department of Statistics at Iowa State University, Ames, Iowa 50011, USA. e-mail: {yifanzhu,maitra}@iastate.edu. F. Dai is with the Department of Mathematical Sciences at the Michigan Technological University, Houghton, Michigan 49931, USA. e-mail: fand@mtu.edu. ©201x IEEE. Personal use of this material is permitted. However, permission to use this material for any other purposes must be obtained from the IEEE by sending a request to pubs-permissions@ieee.org.

Manuscript received xxxx xx,201x; revised xxxxxxxx xx, 201x. First published xxxxxxxx x, xxxx, current version published yyyyyyyy y, yyyy

Digital Object Identifier

where $\mathbf{1}_p = (1, 1, \dots, 1)^{\top}$, and $\mathbf{U} = [\mathbf{u}_1 : \mathbf{u}_2 : \dots : \mathbf{u}_p]$ is a projection matrix, having as its jth column \mathbf{u}_j , the jth anchor point on $\mathbb{S}^1 = \{ \mathbf{x} \in \mathcal{R}^2 : \|\mathbf{x}\| = 1 \}$ for $j = 1, 2, \dots, p$. These p anchor points are equi-spaced on \mathbb{S}^1 . GRadViz uses a transformation $\mathbf{\Psi}(\cdot;\cdot)$ similar to $\mathbf{\Psi}^{\bullet}(\cdot;\cdot)$ in (1) but the anchor points in \mathbf{U} are allowed to lie on a hypersphere \mathbb{S}^q , q > 1 and are not necessarily equi-spaced on \mathbb{S}^q .

As in RadViz2D, our generalization $\Psi(\cdot;\cdot)$ also has a physical interpretation. Suppose that we have p springs connected to the anchor points $u_1, u_2, \ldots, u_p \in \mathbb{S}^q$ and that these p springs have spring constants X_1, X_2, \ldots, X_p . Let $Y \in \mathcal{R}^{q+1}$ be the equilibrium point of the system. Then we have $\sum_{j=1}^p X_j (Y - u_j) = 0$, with our generalization $Y = \Psi(X; U)$ as its solution.

GRadViz is actually a special case of normalized radial visualization (NRV) [18] that allows the anchor points to lie outside the hypersphere and is point-ordering-, line-ordering-, and convexity-invariant. These desirable properties for visualization are also inherited by $\Psi(\cdot;\cdot)$. However, GRadViz is scale-invariant, that is, $\Psi(kX;U) = \Psi(X;U)$ for any $k \neq 0$. In other words, a line passing through the origin is projected to a single point in the radial visualization. So, we need to avoid a situation where all the observations are approximately on a line passing through the origin. The minmax transformation on the jth feature $(j=1,2,\ldots,p)$ of the ith observation

$$m_j(X_{ij}) = \frac{X_{ij} - \min_{1 \le i \le n} X_{ij}}{\max_{1 < i < n} X_{ij} - \min_{1 < i < n} X_{ij}}$$
(2)

guards against this eventuality. It also places every data point in $[0,1]^p$, ensuring that the data, after also applying $\Psi(\cdot;\cdot)$, are all inside the unit ball $\mathbb{B}^{q+1} = \{x \in \mathcal{R}^{q+1} : ||x|| \le 1\}$.

The placement of the anchor points is another issue to be addressed in GRadViz, with different points yielding very different visualizations. Now suppose that X has p uncorrelated coordinates. For any $X_i, X_j \in \mathcal{R}^p$, let $Y_l = \Psi(X_l; U), l \in \{i, j\}$ be the GRadViz-transformed data. The Euclidean distance between Y_i and Y_j is

$$\|\mathbf{Y}_i - \mathbf{Y}_j\|^2 = \left(rac{\mathbf{X}_i}{\mathbf{1}_p^ op \mathbf{X}_i} - rac{\mathbf{X}_j}{\mathbf{1}_p^ op \mathbf{X}_j}
ight)^ op \mathbf{U}^ op \mathbf{U} \left(rac{\mathbf{X}_i}{\mathbf{1}_p^ op \mathbf{X}_i} - rac{\mathbf{X}_j}{\mathbf{1}_p^ op \mathbf{X}_j}
ight),$$

a quadratic form with positive definite matrix $U^{\top}U$ that has the lth diagonal element $u_l^{\top}u_l = 1$ and (k, l)th entry $u_k^{\top}u_l = \cos(u_k, u_l)$. For $X_l = a_l e_l$, with e_l as the lth standard unit vector $(l \in \{i, j\})$,

$$\|\mathbf{Y}_i - \mathbf{Y}_i\|^2 = 2 - 2\cos\langle \mathbf{u}_i, \mathbf{u}_i \rangle. \tag{3}$$

The *i*th and *j*th coordinates of X_i and X_j in this example are as discordant as possible from each other, having perfect negative correlation, and should be placed as far apart as possible (in opposite directions) in the radial visualization. However (3) shows that the distance between Y_i and Y_j approaches 0 as the angle between u_i and u_j approaches 0. Therefore, the radial visualization can create artificial visual correlation between the *i*th and *j*th coordinates if the angle between u_i and u_j is less then $\pi/2$. (As a corollary, strongly positively correlated coordinates should be placed as close together as possible.) To reduce such effects, we need to distribute the anchor points as far away from each other as possible. Therefore, our GRadViz formulation recommends evenly-distributed anchor points on \mathbb{S}^q . RadViz3D has an inherent advantage over RadViz2D because it can more readily facilitate larger angles between anchor points as the smallest angle between any two of p (fixed) evenly-distributed anchor points in RadViz3D is always larger than that in RadViz2D. (Indeed, higher-dimensional displays beyond 3D would be even more beneficial were it possible to obtain such displays.) For example, with p = 4, we can place anchor points in 3D so that the angle between any two of them is the same, but this is not possible in 2D. At the same time, RadViz2D can not place multiple positively correlated coordinates next to each other, as desirable for accurate visualization [19]. The placement of anchor points therefore plays an important role in RadViz2D [20], [21], but is less pronounced with RadViz3D.

Remark 1. Our discussion on GRadViz provides the rationale behind radial visualization with equi-spaced anchor points. It also shows that investigating layouts and spacings, as done [20], [22], [23] for RadViz2D, is unnecessary and perhaps even misleading because of its potential to induce artificial visual correlation between coordinates.

B. Three-dimensional radial visualization

Following the setup and discussion in Section II-A, let $\Psi: \mathbb{R}^p \mapsto \mathbb{B}^3 = \{x \in \mathbb{R}^3: \|x\| \leq 1\}$ map $X \in \mathbb{R}^p$ to $\Psi(X; U) = UX/\mathbf{1}_p^{\top}X$ with U as before and with jth column (anchor point) u_j that, we have contended, should be as evenly-spaced in \mathbb{S}^2 as possible. We find the set \wp of equi-spaced anchor points u_1, u_2, \ldots, u_p from Result 2.

Result 2. Anchor Points Set. Denote the golden ratio by $\varphi = (1+\sqrt{5})/2$. For $p \in \{4,6,8,12,20\}$, the elements in \wp have the coordinates listed in Table I. For other integers $p \geq 5$, only an approximate solution is possible: here the elements of \wp are $\mathbf{u}_j^\top = (u_{j1}, u_{j2}, u_{j3}), j = 1, 2, \ldots, p$ with $u_{j1} = \cos(2\pi j \varphi^{-1})(1 - u_{j3}^2)^{-\frac{1}{2}}, u_{j2} = \sin(2\pi j \varphi^{-1})(1 - u_{j3}^2)^{-\frac{1}{2}}, u_{j3} = (2j-1)/p-1$.

Proof. For $p \in \{4, 6, 8, 12, 20\}$, the coordinates are exactly equi-spaced with anchor points corresponding to the vertices of the Platonic solids. For other values of $p \ge 5$, we derive an approximate solution by implementing a Fibonacci grid method [24] that

TABLE I: Anchor points set for $p \in \{4, 6, 8, 12, 20\}$. Here $\varphi = (1 + \sqrt{5})/2$.

p	Platonic Solid	ρ
4	Tetrahedron	$\{(1,1,1)/\sqrt{3},(1,-1,-1)/\sqrt{3},(-1,1,-1)/\sqrt{3},(-1,-1,1)/\sqrt{3}\}$
6	Octahedron	$\{(\pm 1, 0, 0), (0, \pm 1, 0), (0, 0, \pm 1)\}$
8	Cube	$\{\pm 1,\pm 1,\pm 1\}$
12	Icosahedron	$\{(0,\pm 1,\pm \varphi),(\pm 1,\pm \varphi,0)(\pm \varphi,0,\pm 1)\}/\sqrt{1+\varphi^2}$
20	Dodecahedron	$\left\{ (\pm 1, \pm 1, \pm 1) / \sqrt{3}, (0, \pm \varphi^{-1}, \pm \varphi) / \sqrt{3}, (\pm \varphi^{-1}, \pm \varphi, 1) / \sqrt{3}, (\pm \psi, 0, \pm \varphi^{-1}) / \sqrt{3} \right\}$

produces the latitude ϕ_j and longitude θ_j of the jth anchor point on \mathbb{S}^3 as $\phi_j = \arcsin a_j, \theta_j = 2\pi j \varphi^{-1}$ with a_1, a_2, \ldots, a_p an arithmetic progression chosen to have common difference 2/p. We take $a_1 = 1/p - 1$, so $a_j = 2(j-1)/p + a_1 = (2j-1)/p - 1$. The Cartesian coordinates of the jth anchor point $\mathbf{u}_j \in \wp$ follow by transforming between coordinate systems.

Remark 3. The geometric solutions of \wp for $p \in \{4, 6, 8, 12, 20\}$ are closely related to the Thomson problem in traditional molecular quantum chemistry [25]. Also, for $p \ge 5$, $p \notin \{4, 6, 8, 12, 20\}$, the approximate solution distributes anchor points along a generative spiral on \mathbb{S}^2 , with consecutive points as separated from each other as possible, satisfying the "well-separation" property [26].

Result 2 provides the wherewithal for RadViz3D for $p \geq 4$ by projecting each observation $X_i \in \mathbb{R}^p, i = 1, 2, \dots, n$ to $\Psi(X_i; U = [u_1; u_2; \dots; u_p])$. RadViz3D displays of multidimensional data can then be obtained via 3D graphics to facilitate the discovery of patterns and structure.

III. ILLUSTRATIVE EXAMPLES

We illustrate RadViz3D on some moderately-dimensioned simulated and standard classification datasets and show that it can reveal distinctiveness of class and other structure better than RadViz2D or Viz3D. Because RadViz3D and Viz3D are 3D displays, we only show some of their static views in this paper, referring the reader to the HTML resource for their fuller appreciation. Further, we use the map Ω of pairwise overlap measures [27] to numerically quantify the distinctive of each class relative to the others and compare with our three display methods.

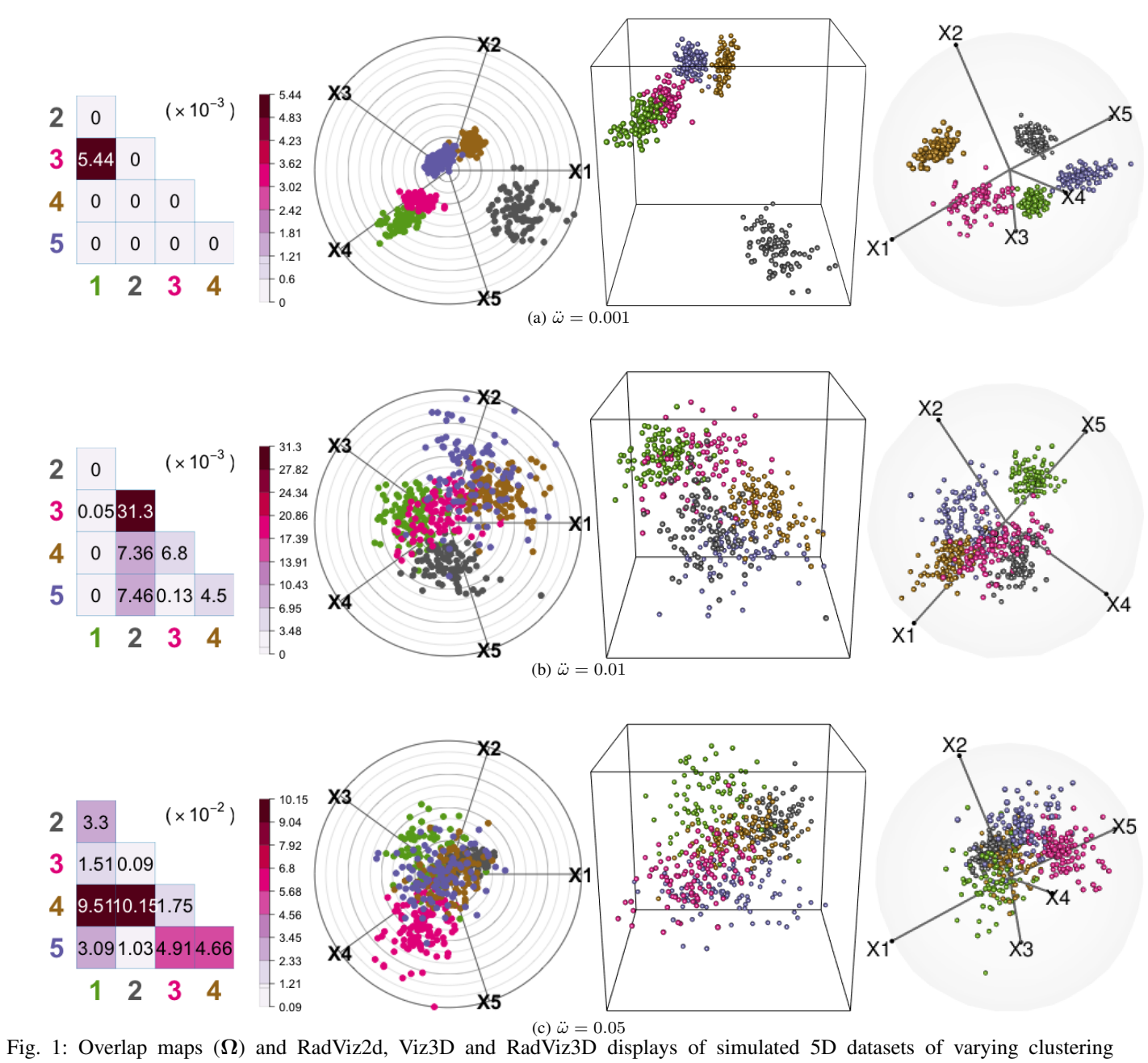
A. Simulated datasets

We simulated 5D datasets of n=500 observations from five groups of known group separation and clustering complexity. The MIXSIM package [28] in R [29] allows for the simulation of class data according to a pre-specified *generalized overlap* $(\ddot{\omega})$ measure [30] that indexes clustering complexity, with a small value $(\ddot{\omega}=10^{-3})$ implying good separation between groups and larger values $(\ddot{\omega}=01,0.05)$ indicating increasingly poorer separation and increased overlap. Fig. 1 displays the results and show that the MIXSIM-generated pairwise overlaps between the 5 groups are essentially preserved in the RadViz3D display. For $\ddot{\omega}=10^{-3}$ (Fig. 1a), the relatively higher overlap between Groups 1 and 3 are captured across all three displays, but unlike RadViz3D, both RadViz2D and Viz3D place both Groups 4 and 5 fairly close together, belying their good separation (and pairwise overlap $\omega_{45}\approx 0$). The more appropriate use of the third dimension by RadViz3D than by Viz3D provides greater benefit at increased $\ddot{\omega}$. For instance, we do not see much qualitative difference in the distinctiveness of the groups between the RadViz2D and Viz3D displays of Figs. 1b and 1c. However, RadViz3D shows that while the five classes are less separated in Fig. 1b than in Fig. 1a, the groups are still fairly distinguishable relative to Fig. 1c. Therefore, the RadViz3D display is seen to provide a more accurate and meaningful representation of the known inherent class structure of these datasets.

B. Real-data examples

We now visualize three multivariate datasets often used in the statistical graphics literature.

- 1) Crabs: This dataset [31] has measurements on morphological characteristics (FL or frontal lip width, RW or rear width, CL or carapace midline length, CW or carapace maximum width, BD or body depth) of 50 crabs each with blue or orange shells and of each gender. Fig. 2 shows the three displays along with the pairwise overlap map Ω . We see less distinction between the males and females as per Ω , but that is not quite captured in the RadViz2D displays (and definitely not so in Viz3D). However, the RadViz3d display indicates that CL may be redundant in the display, as also reported in [32]. Removing this variable results in a clearer display (Fig. 3) where the RadViz3D display shows not just the higher overlap between the blue males and females relative to those between the orange males and females, but also that the species are less distinguishable in terms of these characteristics in the males than in the females. In this illustration, RadViz3D is seen to alone provide important information on the structure of the data in terms of identifying both the redundancy of CL as well as faithful distinction between the classes.
- 2) Wine: This dataset [33] is on the chemical composition of 178 wines from three (Barolo, Gringolino and Barbera) cultivars of grapes grown in the same region of Italy. Fig. 4 provides the three displays of the dataset through the composition of thirteen chemicals: Alcohol (Ahl), Malic acid (Malic), Ash, Alkalinity of ash (Alk), Magnesium (Mg), Total phenols (Pnls), Flavanoids (Flvds), Nonflavanoid phenols (Nonfp), Proanthocyanins (Pthyns), Color intensity, Hue, OD280/OD315 of diluted wines (ODdil) and Proline (Prol). All three displays can not correctly distinguish the first two cultivars from each other but RadViz3D alone separates the third cultivar from the others very well and this matches the overlap measures ($\omega_{13} \approx 0, \omega_{23} \approx 9 \times 10^{-4}$).



complexity $(\ddot{\omega})$. Colors of class labels in Ω are the same for each setting.

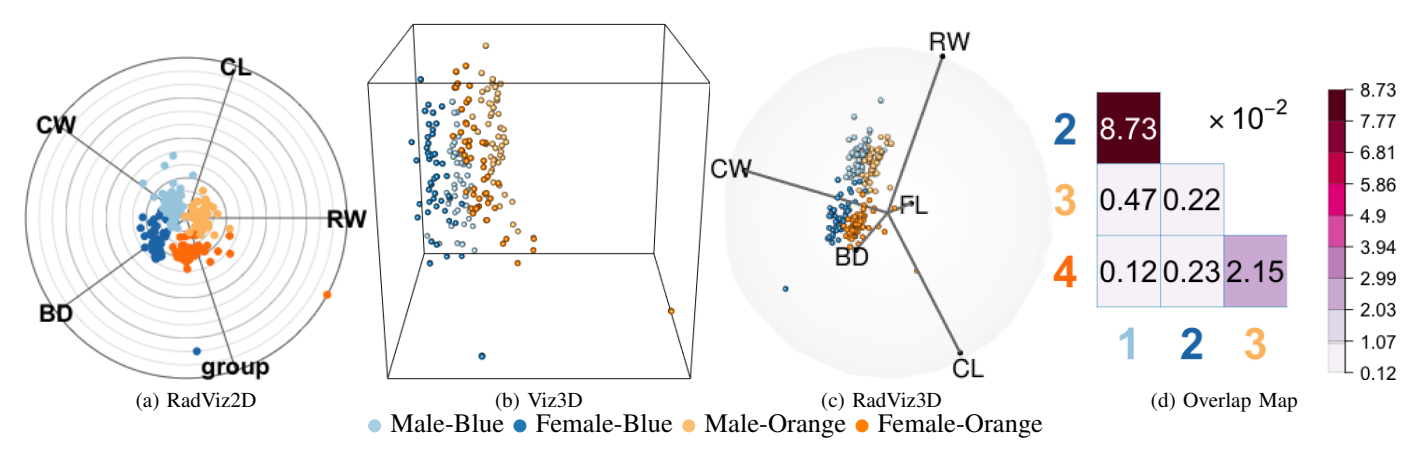


Fig. 2: RadViz2D, Viz3D, RadViz3D displays and overlap map of the Crabs dataset.

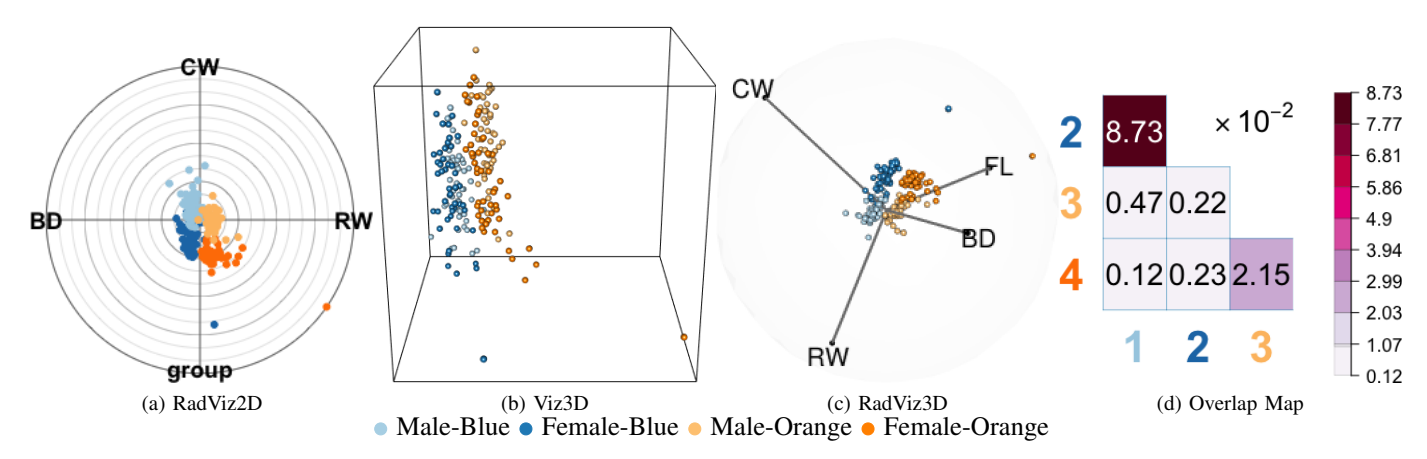


Fig. 3: RadViz2D, Viz3D, and RadViz3D displays and overlap map of the Crabs dataset sans CL.

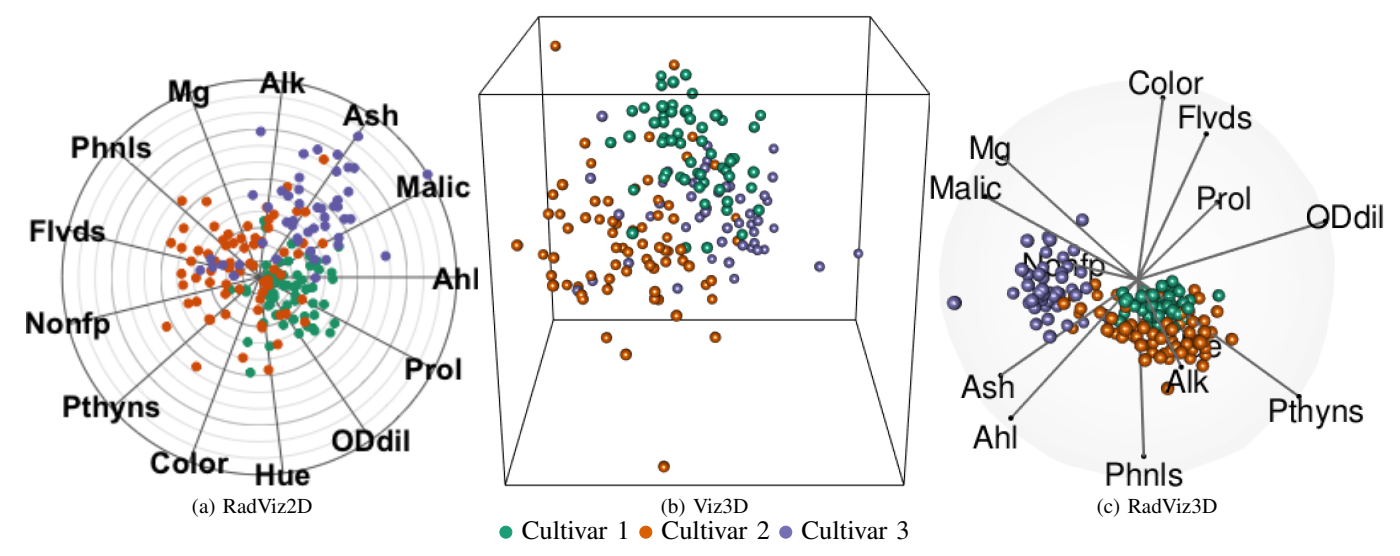


Fig. 4: RadViz2D, Viz3D and RadViz3D displays and overlap map of the Wine dataset.

3) Olive oils: This dataset [34], [35] provides the composition of eight fatty (palmitic, palmitoleic, stearic, oleic, linoleic, linoleic, arachidic, eicosenoic) acids in 572 olive oil samples from nine regions in three areas of Italy. Two regions are (Coastal and Inland) Sardinian, while three (Umbria, East and West Liguria) are from northern Italy and four (North and South Apulia, Calabria, Sicily) are from the South. Fig. 5 shows West Liguria is separated in all three visualizations, but only RadViz3D (Fig. 5d) distinguishes coastal and inland Sardinia from other groups. The northern regions are reasonably distinguished from each other in RadViz3D and well-separated from the other areas (for both 3D methods, though RadViz3D is clearer). The southern regions are difficult to distinguish from each other but more easily distinguished from the north and Sardinia. [36] reported two groups in the southern oils, with North Apulia more distinct than the rest, and our displays (Fig. 5d,e) support this view. Our displays echo [37]'s findings that olive oils are easier distinguished by area than by region.

We end this section by noting that our illustrations show that RadViz3D, with its more meaningful use of the third dimension, can more easily discover structure than either RadViz2D and Viz3D.

IV. DISCUSSION

This short technical note shows that placement of anchor points in a radial visualization plot should ideally be as far away from each other as possible to avoid artificially-induced visual correlations between the coordinates. This desired property motivates our development of a fully 3D radial visualization tool called RadViz3D as it provides for larger distances between anchor points. Our development hinges on our exact and approximate solutions for the placement of p anchor points on the 3D sphere. A R package radviz3d implementing our methodology is publicly available at https://github.com/fanne-stat/radviz3d/, and is demonstrated to accurately reveal class distinctions and lower-dimensional structure in simulated and standard classification datasets.

Some aspects of our development could benefit from further attention. For instance, our development of RadViz3D demonstrates that we should use (at least approximately) equi-spaced anchor points, but the order of the anchor points may still be

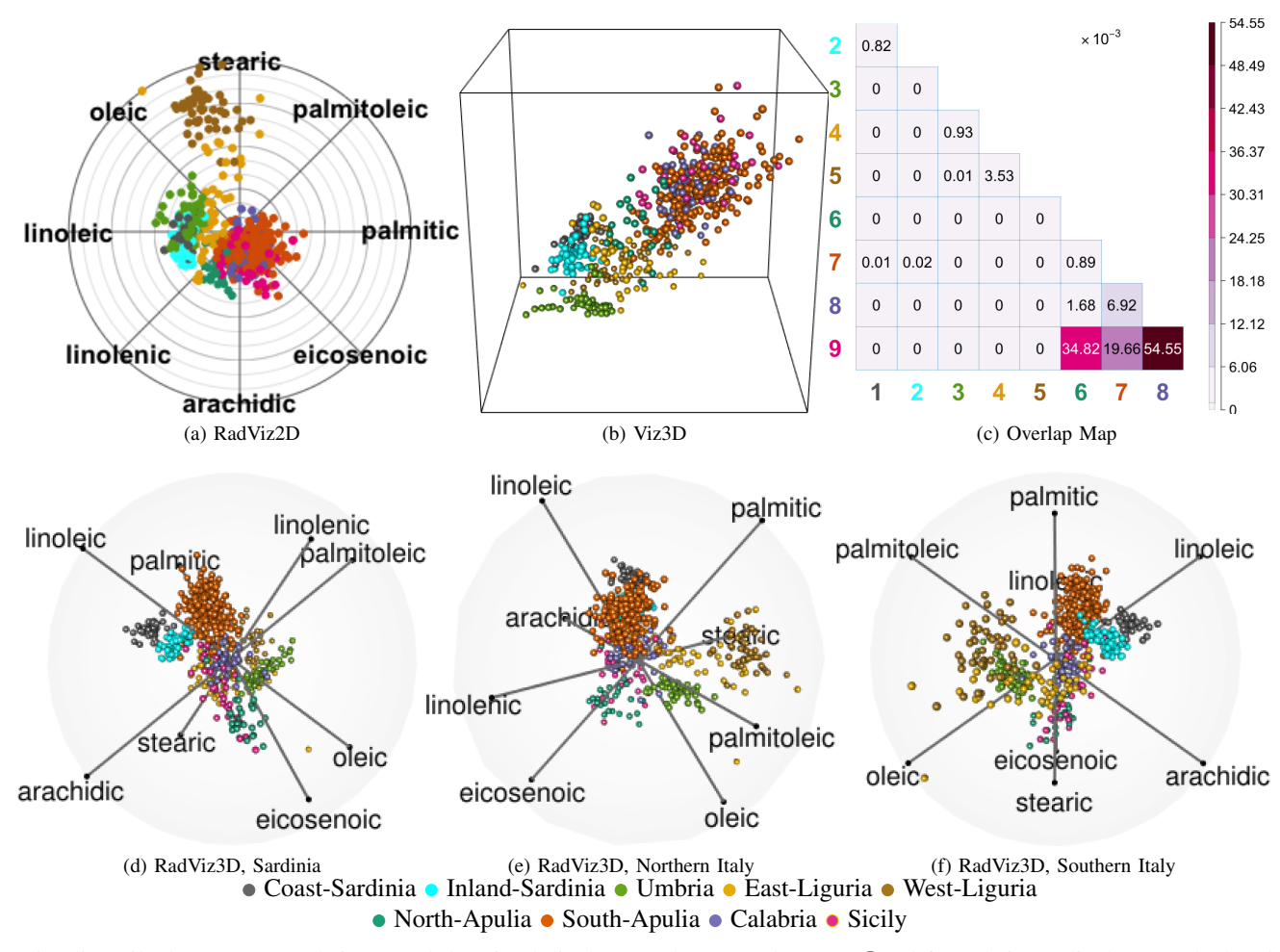


Fig. 5: Olive oils dataset: (a) RadViz2D and (b) Viz3d displays, and (c) Overlap map Ω . (d-f) RadViz3D displays, each showing the distinctiveness of an area's olive oils.

material. The order of anchor points corresponds to switching the order of the columns in the projection matrix U in (1). Clearly different orders of anchor points will produce different visualizations. For the visualization of grouped data, one possible solution to this is to run through all possible orders and pick one that has the biggest separation between groups, where $\ddot{\omega}$ can be used to measure separation. However, this would be very computationally demanding in higher dimensions. Also, based on our assumption that all coordinates are uncorrelated with equi-spaced anchor points, the order is intuitively perhaps not as important since all the coordinates are somewhat equivalent in our display. But it would still be worth getting a definitive answer. Further, for high-dimensional datasets, we will need to look at reducing dimensionality in data before using RadViz3D. Thus, we see that while this paper has made possible fully 3D radial visualization, there remain issues that merit additional investigation.

ACKNOWLEDGMENTS

The authors thank the three reviewers and the Associate Editor for their insightful comments on an earlier version of the manuscript. We also thank N. Kunwar, H. Nguyen, P. Lu, F.S. Aguilar, G. Agadilov and I. Agbemafle for helpful discussions. A version of this manuscript won the first author a 2021 Student Paper Competition award from the American Statistical Association (ASA) Section on Statistical Graphics. The third author's research was supported in part by the United States Department of Agriculture (USDA)/National Institute of Food and Agriculture (NIFA), Hatch project IOW03617. The content of this paper however is solely the responsibility of the authors and does not represent the official views of the USDA.

REFERENCES

- [1] S. K. Card, J. D. Mackinlay, and B. Schneiderman, Readings in information visualization: using vision to think. Morgan Kaufmann, 1999.
- [2] E. Bertini, A. Tatu, and D. Keim, "Quality metrics in high-dimensional data visualization: an overview and systematization," *IEEE Transactions on Visualization and Computer Graphics*, vol. 17, no. 12, p. 2203–2212, 2011.
- [3] J. M. Chambers, W. S. Cleveland, B. Kleiner, and P. A. Tukey, Graphical Methods for Data Analysis. Belmont, CA: Wadsworth, 1983.

- [4] H. Chernoff, "The use of faces to represent points in k-dimensional space graphically," *Journal of the American Statistical Association*, vol. 68, no. 342, pp. 361–368, 1973
- [5] A. Inselberg, "The plane with parallel coordinates," The Visual Computer, vol. 1, pp. 69–91, 1985.
- [6] E. Wegman, "Hyperdimensional data analysis using parallel coordinates," Journal of the American Statistical Association, vol. 85, pp. 664-675, 1990.
- [7] U. Fayyad, G. Grinstein, and A. Wierse, Information Visualization in Data Mining and Knowledge Discovery. Morgan Kaufmann, 2001.
- [8] D. F. Andrews, "Plots of high-dimensional data," Biometrics, vol. 28, no. 1, pp. 125-136, 1972.
- [9] R. Khattree and D. N. Naik, "Andrews plots for multivariate data: Some new suggestions and applications," *Journal of Statistical Planning and Inference*, vol. 100, no. 2, pp. 411–425, 2002.
- [10] K. R. Gabriel, "The biplot graphical display of matrices with application to principal component analysis," Biometrika, vol. 58, pp. 453-467, 1971.
- [11] E. Kandogan, "Visualizing multi-dimensional clusters, trends, and outliers using star coordinates," in *Proceedings of the Seventh ACM SIGKDD International Conference on Knowledge Discovery and Data Mining*, ser. KDD '01. New York, NY, USA: ACM, 2001, pp. 107–116. [Online]. Available: http://doi.acm.org/10.1145/502512.502530
- [12] L. McInnes, J. Healy, N. Saul, and L. Grossberger, "Umap: Uniform manifold approximation and projection," *Journal of Open Source Software*, vol. 3, p. 861, 09 2018.
- [13] P. Hoffman, G. Grinstein, K. Marx, I. Grosse, and E. Stanley, "DNA visual and analytic data mining," in *Proceedings of the 8th conference on Visualization* '97, VIS'97. IEEE Computer Society Press, 1997, p. 437–441.
- [14] P. Hoffman, G. Grinstein, and D. Pinkney, "Dimensional anchors: a graphic primitive for multidimensional multivariate information visualizations," in Proceedings of the 1999 workshop on new paradigms in information visualization and manipulation in conjunction with the eighth ACM internation conference on Information and knowledge management. ACM, 1999, pp. 9–16.
- [15] G. G. Grinstein, C. B. Jessee, P. E. Hoffman, P. J. O'Neil, and A. G. Gee, "High-dimensional visualization support for data mining gene expression data," in DNA Arrays: Technologies and Experimental Strategies, E. V. Grigorenko, Ed. Boca Raton, Florida: CRC Press LLC, 2001, ch. 6, pp. 86–131.
- [16] G. M. Draper, Y. Livnat, and R. F. Riesenfeld, "A survey of radial methods for information visualization," *IEEE Transactions on Visualization and Computer Graphics*, vol. 15, no. 5, pp. 759–776, Sep. 2009.
- [17] A. O. Artero and M. C. F. de Oliveira, "Viz3d: effective exploratory visualization of large multidimensional data sets," in *Proceedings. 17th Brazilian Symposium on Computer Graphics and Image Processing*, Oct 2004, pp. 340–347.
- [18] K. Daniels, G. Grinstein, A. Russell, and M. Glidden, "Properties of normalized radial visualizations," *Information Visualization*, vol. 11, no. 4, pp. 273–300, 2012. [Online]. Available: https://doi.org/10.1177/1473871612439357
- [19] M. Ankerst, D. Keim, and H. P. Kriegel, "Circle segments: a technique for visually exploring large multidimensional data sets," *Human Factors*, vol. 1501, pp. 5–8, 1996.
- [20] L. di Caro, V. Frias-Martinez, and E. Frias-Martinez, "Analyzing the role of dimension arrangement for data visualization in Radviz," in Advances in Knowledge Discovery and Data Mining. Springer, 2010, p. 125–132.
- [21] J. Sharko, G. Grinstein, and K. A. Marx, "Vectorized Radviz and its application to multiple cluster datasets," *IEEE Transactions on Visualization and Computer Graphics*, vol. 14, no. 6, pp. 1444–1451, December 2008.
- [22] T. van Long and V. T. Ngan, "An optimal radial layout for high dimensional data class visualization," in 2015 International Conference on Advanced Technologies for Communications (ATC), 2015, pp. 343–346.
- [23] S. Cheng, W. Xu, and K. Mueller, "Radviz Deluxe: An attribute-aware display for multivariate data," Processes, vol. 5, p. 75, 2017.
- [24] A. González, "Measurement of areas on a sphere using Fibonacci and latitude-longitude lattices," Mathematical Geosciences, vol. 42, p. 49, january 2010.
- [25] M. Atiyah and P. Sutcliffe, "Polyhedra in physics, chemistry and geometry," *Milan Journal of Mathematics*, vol. 71, no. 1, pp. 33–58, Sep 2003. [Online]. Available: https://doi.org/10.1007/s00032-003-0014-1
- [26] E. B. Saff and A. B. Kuijlaars, "Distributing many points on a sphere," The Mathematical Intelligencer, vol. 19, pp. 5-11, dec 1997.
- [27] R. Maitra and V. Melnykov, "Simulating data to study performance of finite mixture modeling and clustering algorithms," *Journal of Computational and Graphical Statistics*, vol. 19, no. 2, pp. 354–376, 2010.
- [28] V. Melnykov, W.-C. Chen, and R. Maitra, "MixSim: An R package for simulating data to study performance of clustering algorithms," *Journal of Statistical Software*, vol. 51, no. 12, pp. 1–25, 2012. [Online]. Available: http://www.jstatsoft.org/v51/i12/
- [29] R Development Core Team, R: A Language and Environment for Statistical Computing, R Foundation for Statistical Computing, Vienna, Austria, 2018, ISBN 3-900051-07-0. [Online]. Available: http://www.R-project.org
- [30] V. Melnykov and R. Maitra, "CARP: Software for fishing out good clustering algorithms," *Journal of Machine Learning Research*, vol. 12, pp. 69 73, 2011.
- [31] N. Campbell and R. Mahon, "A multivariate study of variation in two species of rock crab of the genus leptograpsus," *Australian Journal of Zoology*, vol. 22, no. 3, pp. 417–425, 1974.
- [32] A. E. Raftery and N. Dean, "Variable selection for model-based clustering," *Journal of the American Statistical Association*, vol. 101, pp. 168–178, 2006.
- [33] M. Forina, R. Leardi, and S. Lanteri, "PARVUS an extendible package for data exploration, classification and correlation," Via Brigata Salerno, 16147 Genoa, Italy, 1988.
- [34] M. Forina and E. Tiscornia, "Pattern recognition methods in the prediction of italian olive oil origin by their fatty acid content," *Annali di Chimica*, vol. 72, pp. 143–155, 1982.
- [35] M. Forina, C. Armanino, S. Lanteri, and E. Tiscornia, "Classification of olive oils from their fatty acid composition," in Food Research and Data Analysis. London: Applied Science Publishers, 1983, pp. 189–214.
- [36] I. A. Almodóvar-Rivera and R. Maitra, "Kernel-estimated nonparametric overlap-based syncytial clustering," *Journal of Machine Learning Research*, vol. 21, no. 122, pp. 1–54, 2020.
- [37] A. D. Peterson, A. P. Ghosh, and R. Maitra, "Merging k-means with hierarchical clustering for identifying general-shaped groups," *Stat*, vol. 7, no. 1, p. e172, 2018.